New Zealand Veterinary Journal

Te Hautaka Tākuta Kararehe o Aotearoa

ISSN: 0048-0169 (Print) 1176-0710 (Online) Journal homepage: www.tandfonline.com/journals/tnzv20

Patient-specific three-dimensional-printed models for canine adrenalectomy: a report of three cases

M Rigo, A Pratesi, G Bertolini & F Cinti

To cite this article: M Rigo, A Pratesi, G Bertolini & F Cinti (09 Jun 2025): Patient-specific three-dimensional-printed models for canine adrenalectomy: a report of three cases, New Zealand Veterinary Journal, DOI: 10.1080/00480169.2025.2511195

To link to this article: https://doi.org/10.1080/00480169.2025.2511195

Published online: 09 Jun 2025.

NEW ZEALAND VETERINARY JOURNAL
https://doi.org/10.1080/00480169.2025.2511195

Taylor & Francis
Taylor & Francis Group

CLINICAL STUDY

Patient-specific three-dimensional-printed models for canine adrenalectomy: a report of three cases

M Rigo[a,b], A Pratesi[a], G Bertolini[a] and F Cinti [a]

[a]Surgery Department, San Marco Veterinary Clinic and Laboratory, Veggiano (PD), Italy; [b]Department of Animal Medicine, Production and Health, University of Padua, Legnaro (PD), Italy

ABSTRACT

Case history: Three dogs with adrenal masses scheduled for adrenalectomy were prospectively enrolled into a study to investigate the effectiveness of a 1:1-scale, three-dimensional (3D) printed model of neoplastic adrenal glands to aid surgical planning and provide intra-operative assistance during adrenalectomy in dogs.

Case 1 presented with anorexia, lethargy and a distended abdomen; Case 2 with loss of appetite, behavioural changes, and vocalisation; and Case 3 with mild inappetence during the previous 15 days.

Clinical and imaging findings: On physical examination, mild abdominal pain was noted in all cases. Case 1 was consistently mildly hypertensive over repeated measurements. All cases had mild or moderate elevations in the activities of alanine aminotransferase and aspartate aminotransferase, and the concentration of C-reactive protein. Cases 1 and 2 also had mild leucocytosis. Abdominal CT revealed a left-sided adrenal tumour with caval invasion in Case 1, and right-sided adrenal tumours without caval invasion in Cases 2 and 3. 3D-printed models were created from the CT scan. Different colours were assigned to anatomical structures for better visualisation. Measurements of six anatomical landmarks were made on CT images and on the 3D-printed model. The median absolute difference in measurements taken from the model and the CT scan was 0.75 (min 0, max 3.2) mm.

Treatment and outcome: All dogs underwent surgical removal of the adrenal tumour via sterno-pubic celiotomy. Placing the 3D model on the operating table in the same orientation as the patient allowed for precise pre-planning of the dissection depth. Printed without the fat, and fibrous and capsular tissues that typically cover the retroperitoneal space, the model helped the surgeon to visualise vascular structures that were still covered by connective tissue in the patient. Subjectively, the use of 3D models improved surgical planning and execution by enhancing the understanding of anatomical relationships and enabling the accurate identification of surgical landmarks.

No major intra-operative complications were reported. Post-operative outcomes were favourable, with no significant complications observed.

Clinical relevance: The use of 3D-printed models in adrenal surgeries for dogs may enhance the surgeon's spatial awareness and intra-operative confidence. We recommend that these models are used in conjunction with CT imaging for effective pre-operative planning. Further research with larger sample sizes and a control group would allow a fuller exploration of the benefits of 3D-printed models in veterinary surgical practices.

Abbreviations: ALT: Alanine aminotransferase; AST: Aspartate aminotransferase; CRP: C-reactive protein; CVC: Caudal vena cava; 3D: Three-dimensional

ARTICLE HISTORY
Received 13 November 2024
Accepted 12 May 2025

KEYWORDS
3D printing; adrenalectomy; dog; surgical planning; adrenal tumour; computed tomography

Introduction

The application of three-dimensional (3D) printing in small animal medicine has primarily been limited to the creation of surgical guides for orthopaedic and neurosurgical procedures and custom surgical devices, with only a few reports on its use in soft tissue surgery (Díaz-Regañón *et al.* 2024; Kim *et al.* 2025). In human medicine, however, 3D printing for the creation of phantoms for soft tissue surgery has been more extensively explored (Pietrabissa *et al.* 2020). Regarding adrenal tumours, some studies in human medicine have retrospectively analysed and compared surgical outcomes with and without pre-operative 3D models, with findings suggesting that such models enhance spatial understanding of patient anatomy and provide clearer intra-operative visualisation of tumour–vessel relationships. Subsequent reported benefits include reduced blood pressure fluctuations and shorter surgical time (Zhang *et al.* 2018; Giordano *et al.* 2023; Wang *et al.* 2023).

Right-sided adrenal tumours in dogs are often associated with increased surgical complexity due to their close anatomical relationship with the caudal vena cava (CVC). These tumours are more prone than

CONTACT F Cinti filippocinti@icloud.com

left-sided tumours to invade, or even extend into, the lumen of the CVC, significantly increasing the risk of intra-operative haemorrhage and thrombus-related complications (Jiménez Peláez *et al.* 2008; Barrera *et al.* 2013; Pey *et al.* 2022). Additionally, to minimise the risk of recurrence, surgeons should remove the tumour intact avoiding rupture (Mayhew *et al.* 2023). For this reason, the use of 3D-printed models may be especially valuable in right-sided adrenalectomies, where the proximity to the CVC and its tributaries can make dissection and vascular control particularly challenging. As shown in human surgery, the use of 3D printing in veterinary medicine could offer similar advantages by improving pre-operative planning and intra-operative navigation, potentially leading to safer and more efficient procedures.

To our knowledge, there are no reports on the use of 3D-printed phantoms for pre-operative planning and intra-operative guidance in dogs with adrenal tumours. This study describes the process used to construct 3D-printed models for three dogs with adrenal tumours and their utility for pre-operative planning and intra-operative guidance for adrenalectomy. Additionally, we evaluate the accuracy of the models compared to CT scans.

Case history and clinical findings

The study prospectively enrolled dogs that were presented at the San Marco Veterinary Clinic (Veggiano, Italy) between January 2021 and January 2023 and were diagnosed with adrenal tumours. Owners agreed to abdominal CT scans with pre- and post-contrast phases, followed by adrenalectomy within 1 week of the CT scan. Informed consent of the owners was obtained, but approval of an animal ethics committee was not required as all interventions were part of standard veterinary care.

Three dogs were included in the study. The median weight of the dogs was 20 (min 8, max 29) kg.

Case 1 was a 10-year-old male Jack Russell Terrier that presented with symptoms of anorexia and lethargy persisting for approximately 7 days. On clinical examination, abdominal pain was noted on palpation, and its blood pressure was consistently mildly elevated over repeated measurements. A venous blood sample was collected for a complete blood count and serum biochemistry panel. This revealed elevated liver enzyme activities (alanine aminotransferase (ALT): 431 (reference range 22–52) IU/L; aspartate aminotransferase (AST): 230 (reference range 23–47) U/L), a moderate elevation of the concentration of C-reactive protein (CRP: 67 (reference range 0.1–1.3) mg/L), and mild leukocytosis (24 (reference range 6–17) $\times 10^9$/L).

Case 2 was a 12-year-old neutered male Greyhound that presented with loss of appetite, behavioural changes, and vocalisations. On clinical examination, abdominal pain was noted on palpation. Haematology and serum biochemistry revealed elevated liver enzyme activities (ALT: 171 (reference range 22–52) IU/L; AST: 109 (reference range 23–47) U/L) and the concentration of CRP was mildly elevated at 20.4 (reference range 0.1–1.3 mg/L).

Case 3 was an 11-year-old female Labrador Retriever that presented with mild inappetence for the previous 15 days. On clinical examination, abdominal pain was noted on palpation. Liver enzyme activities were elevated (ALT: 95 (reference range 22–52) IU/L; AST: 49 (reference range 23–47) U/L), as was the concentration of CRP (2.0 (reference range 0.1–1.3) mg/L), and mild leukocytosis (19.3 (reference range 6–17) $\times 10^9$/L) was observed.

Imaging findings

All dogs underwent abdominal ultrasound, which revealed a left-sided adrenal mass in Case 1, and right-sided adrenal masses in Cases 2 and 3. Case 1 also had a mild amount of ascitic fluid and peritoneal reactivity in the region of the neoplasm was observed in Cases 1 and 2.

The dogs then underwent a pre-operative CT scan using a dual-source CT scanner (192 × 2 Somatom Force; Siemens, Erlangen, Germany). As a contrast medium, 2 mL/kg iodixanol (Visipaque 320 mg/ml; GE Healthcare, Chicago, IL, USA), was administered IV, and post-contrast arterial, venous, and portal phases were acquired.

In Case 1, the CT scan revealed a left-sided adrenal mass clearly invading the CVC. The cranial mesenteric artery and left renal vein were near, but not adherent to, the cranial and caudal poles, respectively, of the neoplastic left adrenal gland. In Case 2, the CT scan revealed a right-sided adrenal tumour. There was a mass effect of the tumour against the CVC with irregular margins but no vascular invasion. The tumour was dorsal to the CVC, obscuring the phrenicoabdominal vein, which was fully obstructed by tumour thrombus. In Case 3, the CT scan revealed a right-sided adrenal mass, in contact with the CVC but with smooth margins and no involvement of nearby vessels. The median tumour size measured along its major axis in the CT scan was 4.8 (min 3, max 6) cm.

Production and evaluation of three-dimensional phantom

To enhance our spatial understanding of patient anatomy, facilitate pre-operative planning and improve intra-operative visualisation of tumour–vessel relationships, we constructed 1:1-scale, patient-specific, three-dimensional printed models of each case's adrenal tumour, kidney and associated vasculature.

Three-dimensional phantom design

Computed tomography images in DICOM format were processed using 3D Slicer 5.3.0[1] (Fedorov *et al.* 2012) for organ segmentation to generate stereolithography files. For accurate segmentation, the arterial phase was used to outline the aorta with its branches and the right kidney, while venous and portal phases were employed to delineate the adrenal tumour and the CVC with its venous branches. Four separate stereolithography files were generated, representing arterial components, venous components, the right kidney, and the adrenal mass. Further refinement to eliminate redundant voxels and to smooth the 3D model was carried out using the computer-aided design software Blender (Blender Foundation, Amsterdam, Netherlands). Subsequently, the files were imported into Bambu Studio slicing software (Bambulab, Shenzhen, China), where distinct colours were assigned to each structure: red for arteries, blue for veins, yellow for the kidney, and green for the adrenal mass. The multi-coloured model was printed using polylactic acid filament on a fused deposition modelling printer (X1 Carbon; Bambulab) equipped with a multicolour module.

Tumour grading

Each tumour was classified using a validated seven-point grading system for adrenal tumours (Pey *et al.* 2022) by evaluating the CT scan, the segmented 3D model rendered in Blender, and the 3D-printed model, collectively (Table 1). The grading was performed pre-operatively by both the radiologist (author GB) and the surgeon (author FC) and repeated by the surgeon post-operatively (Table 2).

The radiologist and surgeon graded Case 1's tumour as grade 7, with clear invasion of the CVC.

Table 1. Grading system used to score[a] vascular invasion by adrenal tumours in three dogs that had three-dimensional phantoms of the tumour made to guide surgery (Pey *et al.* 2022).

Grade	Scoring criteria
1	No contact between tumour and vessel (layer of adipose tissue between)
2	Contact between tumour and vessel is <90°; both have smooth margins
3	Contact between tumour and vessel is >90°; tumour border with vessel is concave
4	Contact between tumour and vessel is >90°; tumour border with vessel is convex (i.e. mass effect) and smooth
5	Contact between tumour and vessel; tumour border with vessel is convex (i.e. mass effect) and irregular
6	Tumour compresses vessel such that the point of contact cannot be visualised or the vessel cannot be visualised or is thrombosed
7	Clear invasion of vessel by tumour

[a]The score was assigned by collectively evaluating the CT, the segmented 3D rendering and the 3D-printed model.

Table 2. Scores assigned, based on criteria in Table 1, pre-[a] and post-operatively[b] to the adrenal tumours of three dogs that had three-dimensional phantoms of the tumour made to guide surgery.

	Pre-operative		Post-operative
Case	Surgeon	Radiologist	Surgeon
1	7	7	7
2	5	6	6
3	2	2	2

[a]Score was assigned by surgeon and radiologist collectively evaluating the CT, the segmented 3D rendering and the 3D-printed model.
[b]Score was assigned by surgeon based on their observations during surgery.

Case 2's tumour was graded as grade 5 by the surgeon and grade 6 by the radiologist. For Case 3 the adrenal tumour was graded as grade 2 by both the surgeon and radiologist, showing contact with the CVC but with smooth margins and no involvement of nearby vessels.

Accuracy of three-dimensional phantoms

To evaluate the accuracy of the 3D models, two of the investigators were blinded to patient demographic data and diagnostic information and performed measurements using consistent anatomical landmarks both on the CT scan and the 3D-printed model. We compared measurements of the cranio-caudal length of the mass, the diameter of the CVC at the entrance of the right renal vein, the cranio-caudal kidney axis (left kidney for Case 1, right kidney for Cases 2 and 3), the aorta diameter at the entrance of the right renal artery, the right renal vein diameter at its entrance into the CVC, and the cranial mesenteric artery diameter close to its origin from the aorta. Each measurement was taken three times by each observer; the median value of each landmark is reported in Table 3. The mean absolute difference between measurements taken from the 3D-printed model and the CT scan was 0.81 (min 0, max 3.2) mm, with a median of 0.75 mm. The mean absolute percentage error between measurements from the 3D model and the CT scan was 4.05% (min 0, max 16%) with a median of 3%.

Treatment and outcome

All surgeries were performed by the same board-certified surgeon (author FC) who repeated the grading of the tumour following the surgery (Table 2).

Case 1

Surgery

The dog was positioned in dorsal recumbency. A celiotomy was performed from the xiphoid process to the pubis, continuing lateral to the penis. Abdominal Balfour retractors were used to assist with

[1]https://www.slicer.org/

Table 3. Median measurements (mm) of organ, tumour and vessel landmarks made on CT images and three-dimensional (3D) printed models of the adrenal tumours of three dogs, with percentage absolute difference between 3D and CT measurement.

	Case 1	Case 2	Case 3
Length of mass (CR-CD)			
3D model	49.7	44.5	32.8
CT	50.5	47.8	31.8
Difference (%)	1.6	6.9	3.1
Diameter CVC[a]			
3D model	12.3	16.8	14.1
CT	10.6	17.5	13.4
Difference (%)	16	4.0	5.2
Length of kidney (CR-CD)			
3D model	50.1	93.6	69.3
CT	48.7	92.8	70.3
Difference (%)	2.9	0.85	1.4
Diameter of aorta[b]			
3D model	8.30	13.6	10.9
CT	8.30	13.0	11.7
Difference (%)	0	4.6	6.8
Diameter of right renal vein[c]			
3D model	4.70	9.80	7.10
CT	4.80	8.80	7.23
Difference (%)	2.1	11.4	1.8
Diameter cranial mesenteric artery[d]			
3D model	4.5	6.9	6.6
CT	4.5	7.3	6.73
Difference (%)	0	5.5	1.9

[a]Measured at entrance of right renal vein.
[b]Measured at entrance of right renal artery.
[c]Measured at entrance to CVC.
[d]Measured at origin on aorta.
CR-CD = cranio-caudal; CVC = caudal vena cava.

visualisation. Intra-operatively, based on palpation, the tumour was invading the CVC as shown by the CT scan for about 2 cm cranially. Furthermore, there was a complete invasion of the phrenicoabdominal vein with a tumour thrombus invading the CVC. After complete ligation of the peritumoural vascularisation with a combination of vascular haemoclips (Aesculap; B. Braun, Melsungen, Germany) and a harmonic ultrasound coagulation device (Ethicon Inc, Johnson & Johnson, New Brunswick, NJ, USA), the CVC was temporarily occluded cranially and caudally with tourniquets in respect to the tumour thrombus. The vessel was then sharply opened to retrieve the thrombus and sutured with 5–0 polydioxanone suture. The only intra-operative complications reported were a hypotensive episode during the CVC closure and a modest blood loss (approximately 30 mL) during CVC tourniquet removal. The surgeon graded the tumour post-operatively as grade 7. At the histopathologic examination, the adrenal tumour was identified as an adrenocortical carcinoma.

Three-dimensional model use

The 3D model provided a clear visualisation of the anatomical relationships between the tumour, the cranial mesenteric artery (cranially), and the renal vein (caudally). The model helped to define the correct location of the tourniquets cranial and caudal to the tumour thrombus and aided in deciding the appropriate length of the incision in the wall of the vena cava. Printed without the fat, fibrous and capsular tissue that typically covers the retroperitoneal space, it also helped to identify where specific vascular structures would be located, even before they were directly visualised, effectively aiding in anticipating what would be encountered during the surgical dissection. To facilitate easier identification of the marked vessels in relation to the intra-operative view, the model was placed on the operating table in the same orientation as the patient. All vascular structures were preserved and gently separated from the adjacent tumour during dissection (Figure 1). The main advantage provided by the 3D phantom in this case was, due to the 1:1 scale, the ability to accurately visualise intra-operatively the ideal tourniquet position that had already been calculated pre-operatively based on the CT scan and the model itself. Additionally, observation of the model allowed us to confidently ligate all the vessels supplying the tumour by performing targeted dissection at the exact points where the vessels entered the tumour.

Case 2

Surgery

The dog was positioned in dorsal recumbency. A celiotomy was performed from the xiphoid process to the pubis, continuing lateral to the penis. Abdominal Balfour retractors were used to assist with visualisation. Intra-operatively, the tumour exhibited a mass effect against the CVC. It was positioned almost dorsal to the CVC, obscuring the phrenicoabdominal vein, which was completely filled with tumour thrombus. The renal vein and artery were close but not attached to the tumour. During surgery, the mass appeared to firmly adhere to the wall of the CVC without invading its lumen. The adhesions were removed by blunt dissection, and the peritumoural vascularisation was ligated using a combination of vascular haemoclips (Aesculap; B. Braun) and a harmonic ultrasound coagulation device (Ethicon Inc, Johnson & Johnson). No intra-operative complications were reported. The surgeon graded the tumour post-operatively as grade 6. At the histopathologic examination, the adrenal tumour was identified as a malignant pheochromocytoma.

Three-dimensional model use

As observed for Case 1, using the 3D printed model as a guide, and without the visual interference of fat and connective tissue typically encountered intra-operatively, we were able to anticipate the location of the phrenicoabdominal vein and adjacent vascular structures before encountering them. In this particular case, the model proved especially helpful since the CVC, located dorsally to the tumour, was not initially visible during the procedure. By positioning the model on the operating table in the same orientation

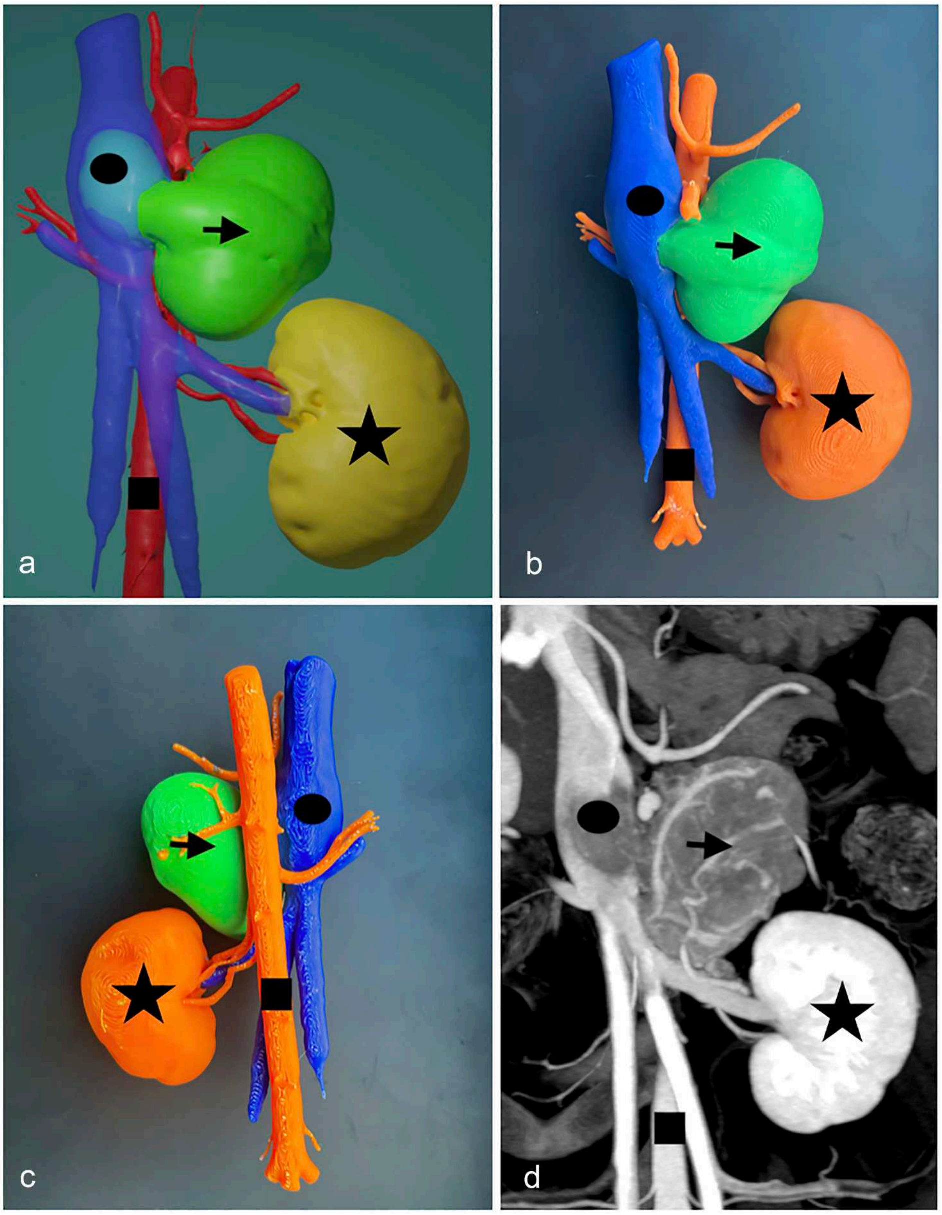

Figure 1. Views of the adrenal tumour of Case 1 showing invasion of the caudal vena cava (CVC) (star: left kidney; square: aorta (caudal trunk); circle: CVC; arrow: adrenal gland tumour): (a) three dimensional (3D) rendering; (b) ventral and (c) dorsal views of the 3D-printed model; (d) post-contrast CT view in a coronal plane. The caval phase was selected to show optimal enhancement of the CVC. Although contrast in the aorta was reduced compared to the early arterial phase, it remained sufficiently visible for anatomical orientation.

as the animal, we were able to pre-plan the appropriate depth for dissection, avoiding accidental injury or rupture of the CVC or phrenicoabdominal vein, which could have occurred with overly aggressive dissection. We were able to accelerate dissection in areas where only the tumour was present and slow down as we approached the CVC and phrenicoabdominal vein, guided by the model's visualisation (Figure 2).

Case 3

Surgery

The dog was positioned in dorsal recumbency. A celiotomy was performed from the xiphoid process to the pubis. Abdominal Balfour retractors were used to assist with visualisation. During surgery, the mass was adhering to the CVC wall, without entering its lumen. The adhesion was removed by blunt dissection and the peritumoural vascularisation was ligated using a combination of vascular haemoclips (Aesculap; B. Braun) and a harmonic ultrasound coagulation device (Ethicon Inc, Johnson & Johnson). No intra-operative complications were reported. The surgeon graded the tumour post-operatively as grade 2. At the histopathologic examination the adrenal tumour was identified as a malignant pheochromocytoma.

Three-dimensional model use

The model, as in previous two cases, proved useful in anticipating the position of the phrenicoabdominal

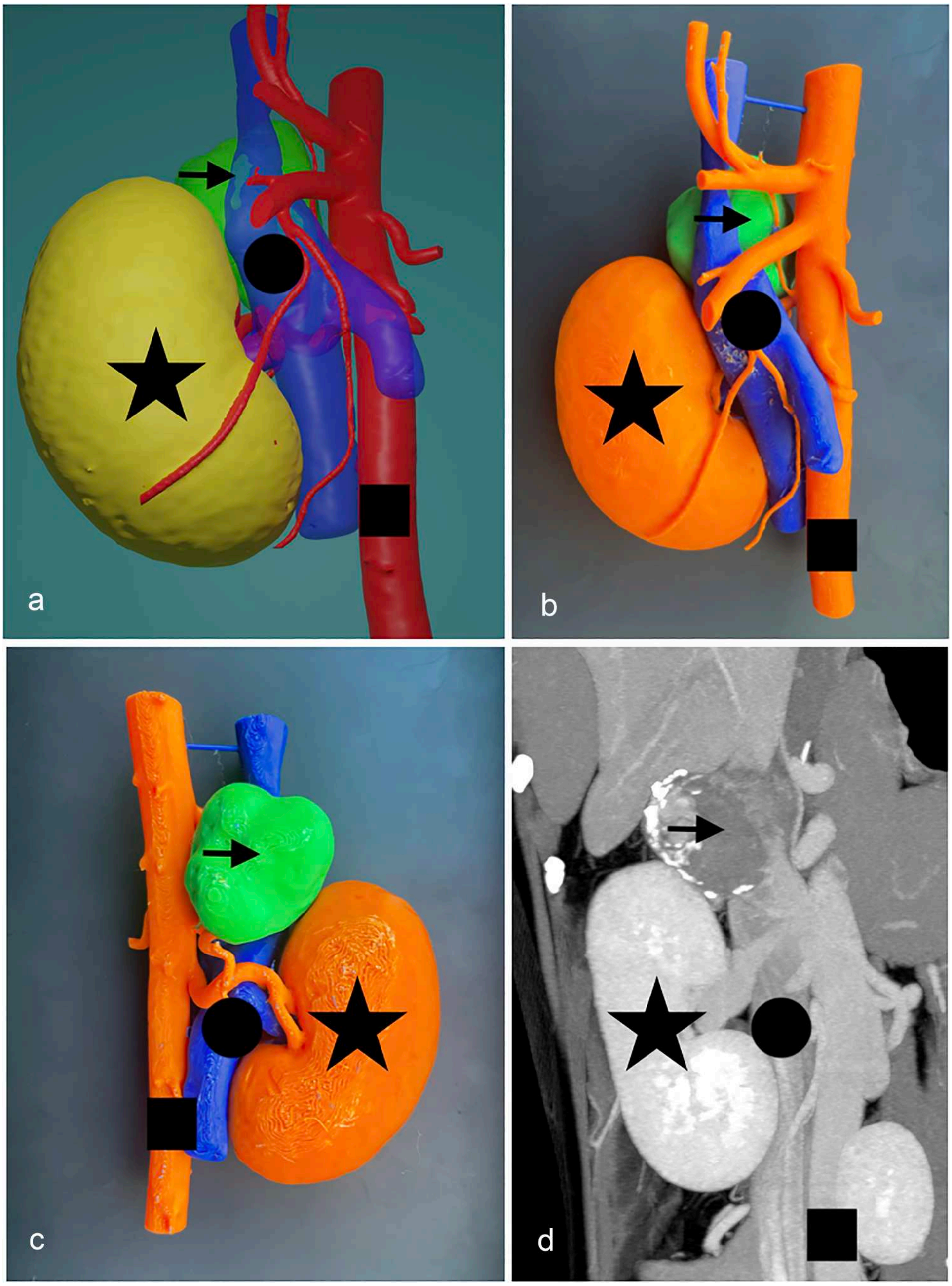

Figure 2. Views of the adrenal tumour of Case 2 (star: right kidney; square: aorta (caudal trunk); circle: caudal vena cava (CVC); arrow: adrenal gland tumour): (a) three dimensional (3D) rendering of right adrenal tumour with CVC adhesion; (b) ventral and (c) dorsal view of the 3D-printed model; (d) post-contrast CT view in a coronal plane. The caval phase was selected to show optimal enhancement of the CVC. Although contrast in the aorta was reduced compared to the early arterial phase, it remained sufficiently visible for anatomical orientation.

vein, which was not thrombosed as in the prior cases. Correctly identifying its position for clipping was crucial to avoid intra-operative haemorrhage. With prior knowledge of its theoretical position, assisted by the model's visualisation, the phrenicoabdomical vein could be located before it was visualised directly. This allowed us to clip the vein promptly and proceed with the rest of the dissection and tumour removal. Compared to the two previous cases involving larger adrenal glands, the model, while extremely helpful, did not provide much additional support regarding the approach to the CVC. In this case, we were able to clearly visualise the CVC, along with the renal vein and arteries (Figure 3).

In both Cases 2 and 3, the 3D printed model provided additional information beyond CT angiography, particularly in terms of tactile spatial comprehension and surgical route rehearsal. The models allowed us to visualise tumour dissection and isolation, which was particularly important in areas where vessels were encased or displaced in unusual ways by the mass. In Case 2, for instance, the model clarified the extent and direction of displacement of the CVC and phrenicoabdominal vessels, allowing a safer surgical approach.

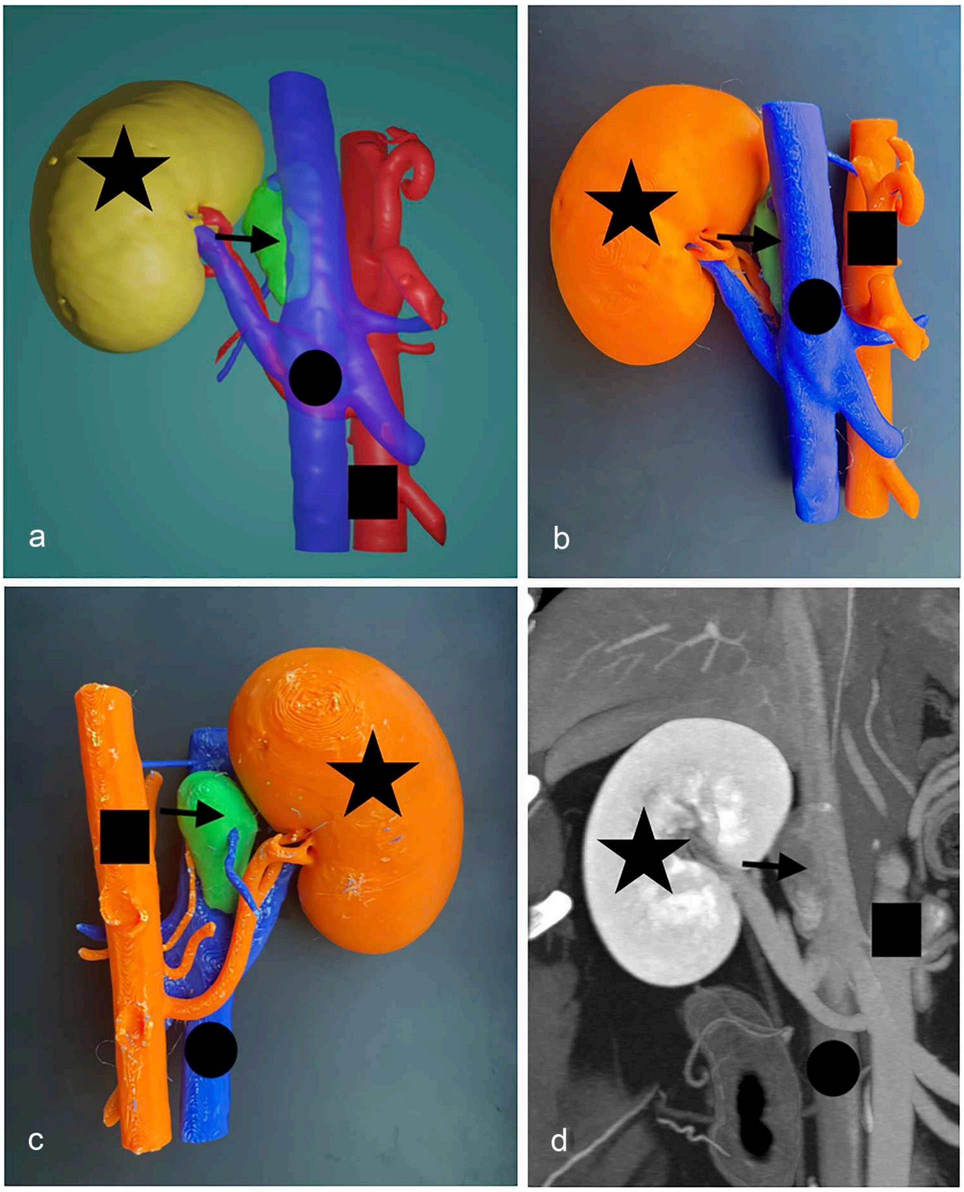

Figure 3. Views of the adrenal tumour of Case 3 (star: right kidney; square: aorta (caudal trunk); circle: caudal vena cava (CVC); arrow: adrenal gland tumour): (a) three dimensional (3D) rendering of right adrenal tumour; (b) ventral and (c) dorsal view of 3D-printed model; (d) post-contrast CT view in a coronal plane. The caval phase was selected to show optimal enhancement of the CVC. Although contrast in the aorta was reduced compared to the early arterial phase, it remained sufficiently visible for anatomical orientation.

We recorded any intra-operative and immediate peri-operative complications within 4 days post-surgery. Complications were classified as minor (not requiring additional surgical intervention) or major (requiring further surgical treatment). No intra-operative or peri-operative complications were recorded in any patient in the first week after surgery.

Discussion

We believe this to be the first published report of the use of a 1:1 scale, 3D-printed model of neoplastic adrenal glands for surgical planning and intra-operative assistance in dogs. The 3D-printed model accurately represented the positions of the main relevant anatomical structures as observed intra-operatively and closely matched measurements taken from the CT scan. The main advantage of the 3D model in this small case series was the ability to provide a simplified and intuitive visual representation of the regional anatomy, which was especially useful intra-operatively to understand the spatial relationships during the procedure and what would be encountered during dissection. The 3D model remained within the surgeon's view, offering a constant, real-time reference throughout the procedure. This reduced the need to rely on memory or prior imaging views. The surgeon reported an increased sense of confidence when planning the surgical approach and managing critical vascular structures. This benefit may be even more pronounced for less experienced surgeons, who could rely more on the 3D model for spatial comprehension, whereas more experienced surgeons might depend primarily on CT imaging. The phantom also aided in correlating anatomical landmarks intra-operatively, making it easy to adapt the surgical strategy in real time.

Another potential advantage of the 3D model is that it displays all structures at once, segmented in various post-contrast phases and ultimately combined into a single model, with each structure clearly indicated by different colours. This allows for the simultaneous viewing of all anatomical features concurrently. With CT reconstruction alone, multiple post-contrast phases may need to be viewed separately, making it more difficult to assess the full spatial relationship between the structures. We did not measure or compare surgical time with that of adrenalectomies performed without the aid of a 3D-printed phantom, as this would require a prospective study specifically designed for that purpose. However, subjectively, the use of the 3D-printed model appeared to facilitate a more efficient surgical procedure and may have contributed to a reduction in intra-operative complications. This observation warrants further investigation in a future controlled study.

The CT scan remains indispensable for its ability to show detailed vascular anatomy and for producing 2D and 3D, multi-planar reconstruction images that provide valuable information for pre-operative planning. It is worth noting that as highlighted by previous studies, CT scans provide only probabilistic information regarding adhesion, which similarly applies to the 3D model since it is derived from 2D CT slices (Rademacher and McAllister 2023). The surgeon's and radiologist's pre-operative grading of the tumours aligned closely, with only a 1-point difference in Case 2. The surgeon's repeated grading after surgery aligned in all three cases with the radiologist's, suggesting that pre-operative imaging provided a consistent reflection of the real intra-operative tumour's characteristics, such as invasiveness and adhesion (Table 2).

Reports in the human literature suggest that 3D-printed models for adrenalectomy planning and intra-operative assistance can be particularly beneficial when considering large tumours with local invasiveness and adhesion to adjacent structures (Zhang *et al.* 2018; Wang *et al.* 2023). This is particularly relevant for right-sided tumours, although, as shown in Case 1 here, large, left-sided tumours can also cause caval invasion. A recent study in humans reported that use of 3D-printed models for planning adrenalectomies for pheochromocytomas is associated with reduced haemodynamic instability. This may be because use of a model allows surgeons to more rapidly ligate the adrenal central vein to control bleeding and catecholamine secretion. Although the timing from surgical incision to central vein ligation was not objectively measured, and remains a subjective observation, it is worth noting that patients operated on with the aid of 3D printed models appeared to experience fewer episodes of blood pressure fluctuation during surgery. This may suggest a smoother intra-operative course, possibly due to more precise pre-operative planning and vessel control (Yao *et al.* 2022). Lastly, employing 3D-printed models in adrenalectomies has been shown to significantly reduce operation times and fluctuations in blood pressure as they help the surgeon to prevent damage to vascular structures (Srougi *et al.* 2016; Wang *et al.* 2023).

Although not evaluated in this study, developing surgical phantoms could be beneficial for pre-operative planning and simulation, particularly for laparoscopic procedures. These models could aid in optimising trocar placement, improving instrument manoeuverability, and identifying vessels to be preserved or ligated. In human medicine, similar models have been studied and shown to enhance surgical planning and rehearsals. They contribute to optimal trocar positioning, better assessment of intra-operative risks, and improved evaluation of margins adjacent to the mass (Souzaki *et al.* 2015; Yao *et al.* 2022; Giordano *et al.* 2023).

There are costs and time requirements associated with creating 3D-printed phantoms. Aside from the cost of (or access to) a 3D printer and design software, the cost of the polylactic acid plastic was US$10–15 for each model in our case series. The design process for each model took 6–10 hours, with practice reducing the time needed, and the 3D-printing process required 24–36 hours.

This study was limited by its small sample size; a larger cohort could have provided more extensive data for a deeper exploration of the benefits of 3D printing in preparing for complex surgeries. Additionally, it is noteworthy that there was no comparison with surgeries performed without the assistance of a 3D-printed model. Evaluating differences in variables such as blood loss, procedural duration, and overall outcomes between surgeries using the 3D-printed adrenal model and those without it would be valuable. If these models are to be used in the future for laparoscopic surgical simulations, it will be essential to develop suitable materials that accurately replicate the tissue characteristics of various organs, such as elasticity, softness, and tension.

In conclusion, the 3D-printed model was shown to correlate well with both the CT scan images and the intra-operative findings and could be a useful addition for planning of the surgical intervention. It should be noted that the 3D-printed model simplifies details from the CT scan, and it cannot accurately replicate microvasculature and tissue adhesions. While the model is useful intra-operatively, and can give an excellent overall spatial awareness, the CT scan remains essential for evaluating vascular anatomy; for this reason, the 3D model should be used as an adjunct, not a replacement for CT, in surgical planning. Lastly, sourcing or developing materials that provide a more realistic pre-operative simulation would be worthwhile.

Disclosure statement

No potential conflict of interest was reported by the author(s).

ORCID

F Cinti http://orcid.org/0000-0003-1680-0523

References

Barrera JS, Bernard F, Ehrhart EJ, Withrow SJ, Monnet E. Evaluation of risk factors for outcome associated with adrenal gland tumors with or without invasion of the caudal vena cava and treated via adrenalectomy in dogs: 86 cases (1993–2009). *Journal of the American Veterinary Medical Association* 242, 1715–21, 2013. https://doi.org/10.2460/javma.242.12.1715

Díaz-Regañón D, Mendaza-De Cal R, García-Sancho M, Rodríguez-Franco F, Sainz Á, Rodriguez-Quiros J, Rojo C. Canine upper digestive tract 3D model: assessing its utility for anatomy and upper endoscopy learning. *Animals* 14, 1070, 2024. https://doi.org/10.3390/ani14071070

Fedorov A, Beichel R, Kalpathy-Cramer J, Finet J, Fillion-Robin J-C, Pujol S, Bauer C, Jennings D, Fennessy FM, Sonka M, *et al*. 3D slicer as an image computing platform for the quantitative imaging network. *Magnetic Resonance Imaging* 30, 1323–41, 2012. https://doi.org/10.1016/j.mri.2012.05.001

Giordano A, Moroni F, Filippo GD, Cammelli F, Guagni T, Perini D, Cantafio S. Laparoscopic adrenalectomy for large adrenal tumor guided by a 3D anatomic model. New frontiers in abdominal surgery. *Journal of Surgical Case Reports* 2023, rjad104, 2023. https://doi.org/10.1093/jscr/rjad104

Jiménez Peláez M, Bouvy BM, Dupré GP. Laparoscopic adrenalectomy for treatment of unilateral adrenocortical carcinomas: technique, complications, and results in seven dogs. *Veterinary Surgery* 37, 444–53, 2008. https://doi.org/10.1111/j.1532-950X.2008.00410.x

Kim T, Jeon Y, Kim Y, Kymm VT, Kim S, Lee D, Roh Y. Comparison of accuracy of brain biopsy simulation between 3-dimensional–printed guides and neuronavigation in skull-brain tumor models of dogs and cats. *American Journal of Veterinary Research* 86, ajvr.24.10.0301, 2025. https://doi.org/10.2460/ajvr.24.10.0301

Mayhew PD, Massari F, Araya FL, Van Nimwegen SA, Van Goethem B, Singh A, Balsa IM, Steffey MA, Culp WTN, Case JB, *et al*. Laparoscopic adrenalectomy for resection of unilateral noninvasive adrenal masses in dogs is associated with excellent outcomes in experienced centers. *Journal of the American Veterinary Medical Association* 261, 1–8, 2023. https://doi.org/10.2460/javma.23.03.0135

Pey P, Specchi S, Rossi F, Diana A, Drudi I, Zwingenberger AL, Mayhew PD, Pisoni L, Mari D, Massari F, *et al*. Prediction of vascular invasion using a 7-point scale computed tomography grading system in adrenal tumors in dogs. *Journal of Veterinary Internal Medicine* 36, 713–25, 2022. https://doi.org/10.1111/jvim.16371

Pietrabissa A, Marconi S, Negrello E, Mauri V, Peri A, Pugliese L, Marone EM, Auricchio F. An overview on 3D printing for abdominal surgery. *Surgical Endoscopy* 34, 1–13, 2020. https://doi.org/10.1007/s00464-019-07155-5

Rademacher N, McAllister H. Abstracts from the 2023 IVRA EVDI Joint Scientific Conference Dublin, Ireland, June 18–23, 2023. *Veterinary Radiology and Ultrasound* 64, 1113–54, 2023. https://doi.org/10.1111/vru.13289

Souzaki R, Kinoshita Y, Ieiri S, Kawakubo N, Obata S, Jimbo T, Koga Y, Hashizume M, Taguchi T. Preoperative surgical simulation of laparoscopic adrenalectomy for neuroblastoma using a three-dimensional printed model based on preoperative CT images. *Journal of Pediatric Surgery* 50, 2112–5, 2015. https://doi.org/10.1016/j.jpedsurg.2015.08.037

Srougi V, Rocha BA, Tanno FY, Almeida MQ, Baroni RH, Mendonça BB, Srougi M, Fragoso MC, Chambô JL. The use of three-dimensional printers for partial adrenalectomy: estimating the resection limits. *Urology* 90, 217–21, 2016. https://doi.org/10.1016/j.urology.2015.11.043

Wang Y, Liu L, Pang Y, Chen D, Xu X, Liu J, Guan X. Nomogram for predicting hemodynamic instability and the association between preoperative 3D printing and hemodynamic instability during laparoscopic adrenalectomy for pheochromocytoma. *American Journal of Cancer Research* 13, 1602–10, 2023

Yao XW, Ai K, Li Y. Presurgical planning of 3D printing for a large abdominal pheochromocytoma and paraganglioma. *Urology* 165, 356–8, 2022. https://doi.org/10.1016/j.urology.2022.04.033

Zhang B, Chen Z, Hu X, He Y, Li M, Liu P, Du Y, Liu Y, Chen X. Application of three-dimensional visualization technology in laparoscopic surgery for pheochromocytoma/paraganglioma: a single-center experience. *Journal of Laparoendoscopic and Advanced Surgical Techniques* 28, 997–1002, 2018. https://doi.org/10.1089/lap.2017.0704